PHYSICAL REVIEW B **86**, 241103(R) (2012)

Correlation between *p*-type conductivity and electronic structure of Cr-deficient $CuCr_{1-x}O_2$ ($x = 0$–0.1)

Shashi B. Singh,[1] L. T. Yang,[1] Y. F. Wang,[1] Y. C. Shao,[1] C. W. Chiang,[1] J. W. Chiou,[2] K. T. Lin,[1,*] S. C. Chen,[1] B. Y. Wang,[1] C. H. Chuang,[1] D. C. Ling,[1,†] W. F. Pong,[1,‡] M.-H. Tsai,[3] H. M. Tsai,[4] C. W. Pao,[4] H. W. Shiu,[4] C. H. Chen,[4] H.-J. Lin,[4] J. F. Lee,[4] H. Yamane,[5] and N. Kosugi[5]

[1]*Department of Physics, Tamkang University, Tamsui 251, Taiwan*

[2]*Department of Applied Physics, National University of Kaohsiung, Kaohsiung 811, Taiwan*

[3]*Department of Physics, National Sun Yat-Sen University, Kaohsiung 804, Taiwan*

[4]*National Synchrotron Radiation Research Center, Hsinchu 300, Taiwan*

[5]*Institute for Molecular Science, Okazaki 444-8585, Japan*

(Received 1 August 2012; published 7 December 2012)

The correlation between the *p*-type hole conduction and the electronic structures of Cr-deficient $CuCr_{1-x}O_2$ ($x = 0$–0.1) compounds was investigated using O *K*-, Cu, and Cr $L_{3,2}$-edge x-ray absorption near-edge structure (XANES), scanning photoelectron microscopy, and x-ray emission spectroscopy measurements. XANES spectra reveal a gradual increase in the Cu valence from Cu^{1+} to Cu^{2+} with increasing Cr deficiency x, whereas, the valence of Cr remains constant as Cr^{3+}. These results indicate that the *p*-type conductivity in the $CuCr_{1-x}O_2$ samples is enhanced by a Cu^{1+}-O-Cu^{2+} rather than a Cr^{3+}-Cr^{4+} or direct Cu^{1+}-Cu^{2+} hole mechanism. Remarkable Cr-deficiency-induced changes in the densities of Cu 3*d*, Cu 3*d*-O 2*p*, and O 2*p* states at or near the valence-band maximum or the Fermi level were also observed. In addition, a crossover of conduction mechanism from thermally activated (TA) hopping to a combination of TA and Mott's three-dimensional variable range hopping occurs around 250 K.

DOI: 10.1103/PhysRevB.86.241103 PACS number(s): 78.70.Dm, 73.25.+i, 73.23.−b

Delafossite oxides, $CuMO_2$ (M = trivalent metal cations), have recently attracted much interest because of their intriguing magnetoelectric properties, making them promising candidates for new optoelectronic and spin-based device applications.[1,2] These compounds contain a two-dimensional triangular lattice composed of $M^{3+}O_2$ in which the layers of edge-sharing MO_6 octahedra lie parallel to the *ab* plane; the Cu^{1+} ions are linearly connected to two O ions that are alternately stacked along the *c* axis[3] (see the Supplemental Material of Fig. S1 in Ref. 4). Among them, $CuCrO_2$ has attracted considerable attention due to its favorable transport properties. It has been suggested that the observed higher conductivity of $CuCrO_2$ than that of other delafossites may arise from the mixing of Cr 3*d* and O 2*p* states in the Cr^{3+}-O-Cu^{1+} linkages.[5] Theoretical calculations using the augmented spherical wave method showed that the density of states (DOS) of $CuCrO_2$ at or near the valence-band maximum (VBM) or the Fermi level (E_f) is composed mainly of the Cr 3*d* orbitals,[6] indicative of a Cr^{3+}-Cr^{4+} hole mechanism. It can account for the increase in conductivity observed in $CuCr_{1-x}Mg_xO_2$ compounds where Cr^{4+} holes are formed by the substitution of Mg^{2+} in the matrix of Cr^{3+}.[7] Subsequently, calculations based on density-functional theory showed that the Cu and Cr 3*d* states at or near VBM or E_f exhibit a strong covalent interaction with O 2*p* states, forming delocalized holes in $CuCrO_2$ and yielding high electronic conductivity.[8–10] However, more recent theoretical studies by Scanlon and Watson proposed that the Cu^{1+}-Cu^{2+} hole mechanism is more prominent than the Cr^{3+}-Cr^{4+} hole mechanism in $CuCrO_2$.[11] They also showed that the DOS at the VBM or E_f is composed mainly of the Cu 3*d* states in $CuCrO_2$. Experimentally, x-ray emission spectroscopy (XES) revealed that the DOS at the top of the valence band in the Cu-based delafossites is dominated by the Cu 3*d* character.[12]

More recently, Ling *et al.* found that Cr deficiency increases conductivity by more than 2 orders of magnitude in Cr-deficient $CuCr_{1-x}O_2$ ($x = 0$–0.1) compounds.[13] They also reported that the Seebeck coefficient is positive, confirming that the *p*-type holes govern the transport in these compounds. Despite the extensive investigations mentioned above, the relevant path responsible for the *p*-type hole conduction remains controversial. To address this issue, x-ray absorption near-edge structure (XANES), extended x-ray absorption fine structure (EXAFS), valence-band photoemission spectroscopy (VB-PES), and XES were employed to elucidate the correlation between the electronic or atomic structures and the *p*-type conductivity of the Cr-deficient $CuCr_{1-x}O_2$ ($x = 0$–0.1) compounds. The samples studied were prepared by the standard solid-state reaction. Their structural, transport, and magnetic properties have been characterized in detail elsewhere.[13] XANES, EXAFS, VB-PES, and XES experiments have also been described in detail in the Supplementary Material.[4] The results clearly reveal that the hole-conduction mechanism involves Cu^{1+}-O-Cu^{2+} rather than Cr^{3+}-Cr^{4+} or direct Cu^{1+}-Cu^{2+} paths.

Figure 1(a) presents normalized O *K*-edge XANES spectra of the $CuCr_{1-x}O_2$ ($x = 0$–0.1) samples and the Cu_2O, CuO, Cr_2O_3, and CrO_2 references at room temperature (RT). Since the surface of CrO_2 is easily contaminated with Cr_2O_3,[14] the O *K*-edge XANES spectrum of reference CrO_2 was taken from the literature.[15] Note that the features of the references are consistent with those reported elsewhere.[14–16] The general line shape and threshold energy of the O *K*-edge XANES spectra of $CuCr_{1-x}O_2$ differ from those of reference CuO and CrO_2. The spectra of the $CuCr_{1-x}O_2$ samples display four major near-edge features, labeled A_1–D_1, which are centered at ~530, 533, 535, and 542 eV, respectively. These features provide detailed

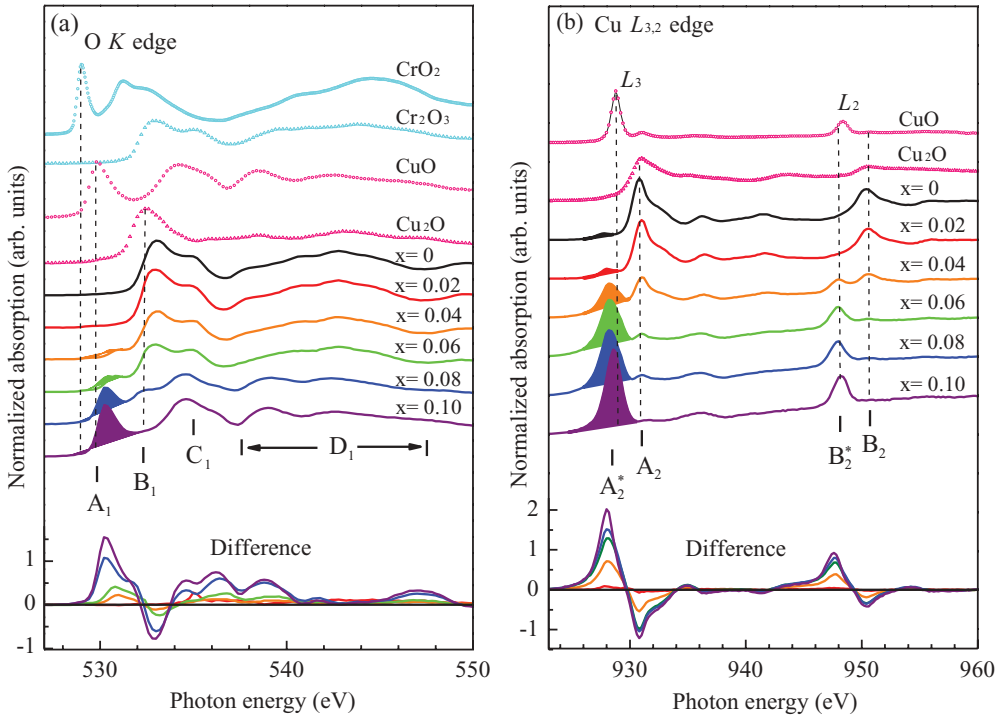

FIG. 1. (Color online) (a) O K-edge XANES spectra of samples studied and the CrO_2, Cr_2O_3, CuO, and Cu_2O reference materials. The bottom panel shows the difference in spectra of $CuCr_{1-x}O_2$ samples between $x = 0.02-0.1$ and $x = 0$. (b) Cu $L_{3,2}$-edge XANES of $CuCr_{1-x}O_2$ and reference CuO and Cu_2O samples. The bottom panel shows the difference in spectra of $CuCr_{1-x}O_2$ samples between $x = 0.02-0.1$ and $x = 0$.

information about unoccupied O $2p$-derived states above E_f in $CuCr_{1-x}O_2$. The main general features at the O K edge for the low Cr-deficient ($x = 0$ and 0.02) samples is similar to that of the superposed spectra of Cr_2O_3 and Cu_2O with a dominant contribution from Cr_2O_3. They include three features, B_1–D_1, which are attributable to O $2p$ states that are hybridized with Cr/Cu $3d$ and $4sp$ states. Specifically, features B_1 and C_1 are attributable mostly to the O $2p$-Cr $3d$ hybridized states with a small contribution from O $2p$-Cu $3d$ hybridized states based on the theoretical calculations for $CuCrO_2$.[8,9] Feature A_1 centered at ~530 eV, which is also observed in the CuO spectrum, emerges as x increases from 0.04 to 0.1. The bottom of Fig. 1(a) presents the difference in spectra between the $x = 0.02 - 0.1$ and $x = 0$ samples. Note that the intensity variation in feature A_1 is opposite that of feature B_1 with increasing Cr deficiency. It suggests that the O K-edge XANES spectral feature is dominated by O $2p$ and Cu^{1+}/Cr^{3+} $3d$ hybridized states for the low Cr-deficient samples with $x = 0$ and 0.02 and then by O $2p$ and Cu^{2+}/Cr^{3+} $3d$ hybridized states for the high Cr-deficient samples with $x = 0.04 - 0.1$. As x increases, the emergence of feature A_1, accompanied by the reduction of the intensity of feature B_1, is caused by the formation of unoccupied O $2p$-Cu^{2+} $3d$ hybridized states, indicative of the presence of excess holes at the O sites due to the generation of Cu^{2+}.[17,18] Furthermore, the absence of a sharp feature at ~529 eV, associated with CrO_2 in the spectra of the samples studied, suggests that the O $2p$-Cr^{4+} $3d$ hybridized states may not exist in the $CuCr_{1-x}O_2$ samples.

Figure 1(b) displays the normalized Cu $L_{3,2}$-edge XANES spectra of $CuCr_{1-x}O_2$ ($x = 0-0.1$) and reference CuO and Cu_2O at RT. The bottom panel of Fig. 1(b) presents the difference in spectra between the $x = 0.02 - 0.1$ and the $x = 0$ samples. It includes two dominant features, A_2^*/A_2 and B_2^*/B_2, in the energy range of 924–936 eV and 942–956 eV, which, by the dipole-transition selection rules, correspond to Cu L_3 ($2p_{3/2} \rightarrow 3d$) and L_2 ($2p_{1/2} \rightarrow 3d$) transitions, respectively. The main feature in the Cu $L_{3,2}$-edge XANES spectra of the $CuCr_{1-x}O_2$ samples changes significantly as x increases. The low Cr deficiency samples with $x \leqslant 0.02$ have similar spectral features to that of Cu_2O (Cu^{1+}) with dominant features A_2 and B_2 at the L_3 and L_2 edges, respectively, which supports the dominance of the Cu^{1+} valence in the low Cr-deficient samples with $x = 0$ and 0.02. As x increases from 0.04 to 0.1, features A_2^* and B_2^* appear at the Cu $L_{3,2}$ edge, and a similar characteristic feature is observed in the CuO (Cu^{2+}) spectrum. The observed changes in the spectral features at the Cu $L_{3,2}$ edge confirm the gradual change in the Cu valence from Cu^{1+} to Cu^{2+} as x increases from 0 to 0.1 in the $CuCr_{1-x}O_2$ samples. This result is consistent with that of the O K-edge XANES shown in Fig. 1(a), suggesting that the gradual change in the Cu valence from Cu^{1+} to Cu^{2+} with increasing Cr deficiency is caused by the generation of excess holes at the Cu sites ($Cu^{2+}/Cu^{1+}\underline{L}$, $\underline{L}$ denotes the O $2p$ ligand hole), which are linked to the O sites arising from the strong hybridization between Cu $3d$ and O $2p$ states in the $CuCr_{1-x}O_2$ compounds.

Figure 2(a) presents the Cr $L_{3,2}$-edge XANES spectra of the samples investigated and the Cr_2O_3 and CrO_2 (the spectrum referred by Ref. 15) at RT. The bottom panel of Fig. 2(a) shows the difference in spectra of $CuCr_{1-x}O_2$ samples between $x = 0.02 - 0.1$ and $x = 0$. Since the energy separation between

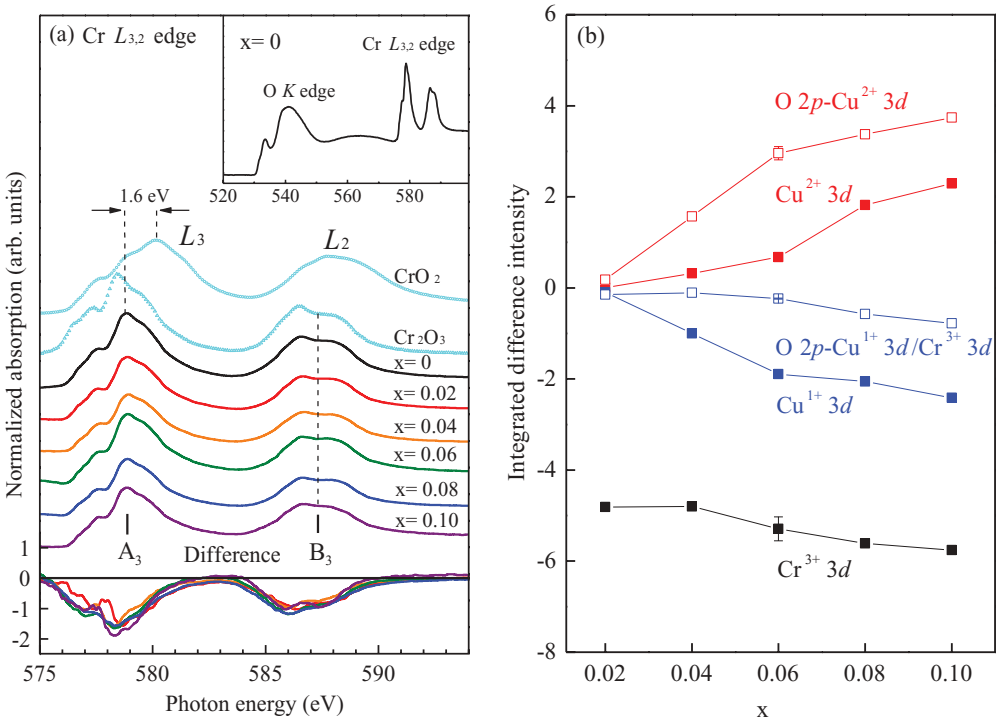

FIG. 2. (Color online) (a) Cr $L_{3,2}$-edge XANES spectra of samples studied and the CrO_2 and Cr_2O_3 reference materials. The upper inset shows O K- and Cr L_3-edge XANES spectra of the $x = 0$ sample. The bottom panel presents the difference in the spectra of the $CuCr_{1-x}O_2$ samples between $x = 0.02 - 0.1$ and $x = 0$. (b) Integrated difference intensities of O K-, Cu, and Cr L_3-edge XANES spectra of $CuCr_{1-x}O_2$ versus the Cr deficiency.

the O K and the Cr L_3 edge in the $CuCr_{1-x}O_2$ spectrum is approximately 50 eV, as presented in the upper inset of Fig. 2(a), the Cr $L_{3,2}$-edge XANES was carefully normalized by matching the absorption coefficients in the region from 2 eV below the L_3 edge to 10 eV above the L_2 edge and was kept in the same area in the energy range between 595 and 598 eV to avoid a mix up with the O K postedge absorption. Notably, both spectra of $CuCr_{1-x}O_2$ and Cr_2O_3 exhibit dominant broad features, A_3 and B_3, centered at ~579 and 587 eV, which are attributable to Cr L_3 ($2p_{3/2} \rightarrow 3d$) and L_2 ($2p_{1/2} \rightarrow 3d$) transitions, respectively. The general spectral features in the $CuCr_{1-x}O_2$ samples bear a resemblance to those of Cr_2O_3 (Cr^{3+}) rather than CrO_2 (Cr^{4+}) and the dominant broad features A_3 and B_3 of $CuCr_{1-x}O_2$ shift to lower energy by ~1.6 eV than those of CrO_2, indicating the dominance of the Cr^{3+} oxidation state and an absence of the Cr^{4+} valence in the $CuCr_{1-x}O_2$ samples. This finding is consistent with the result deduced from the O K-edge XANES spectra described above.

Figure 2(b) plots the integrated difference intensities of features A_1 (O 2p-Cu^{2+} 3d) and B_1 (O 2p-Cu^{1+}/Cr^{3+} 3d) at the O K edge, features A_2^* (Cu^{2+}) and A_2 (Cu^{1+}) at the Cu L_3 edge, and feature A_3 (Cr^{3+}) at the Cr L_3-edge XANES spectra as a function of the Cr deficiency x. The intensities of the features associated with the O 2p-Cu^{1+}/Cr^{3+} 3d hybridized states and the Cu^{1+} 3d valence states gradually decrease, those of the features associated with the O 2p-Cu^{2+} 3d hybridized states in the O K-edge spectra and the Cu^{2+} valence states in the Cu L_3-edge spectra increase, and those of the features associated with the Cr^{3+} valence states derived from the Cr L_3-edge spectra decrease as x increases. The results shown in Fig. 2(b) along with the temperature-dependent Cr $L_{3,2}$-edge XANES spectra (see the Supplementary Material of Fig. S2 in Ref. 4) unambiguously show the absence of the Cr^{4+} valence in the $CuCr_{1-x}O_2$ compounds. It rules out the Cr^{3+}-Cr^{4+} hole mechanism as a possible scenario for transport properties of samples studied. In contrast, the underlying origin of the p-type conduction in the $CuCr_{1-x}O_2$ samples is, therefore, hole doping at the Cu/O sites. These excess holes are expected to hop from one Cu to another Cu site through a process of Cu^{1+} 3d-O 2p-Cu^{2+} 3d. The variations in the intensities with increasing Cr deficiency inferred from the O K-, Cu, and Cr L_3-edge spectra suggest that the enhanced p-type conduction is associated with the *itinerant* "hole doping" and "electron transfer" from the Cu 3d orbitals through the Cu^{1+}-O-Cu^{2+} dumbbell bridges to the $Cr^{3+}O_2$ octahedral layers, acting as a reservoir for electrons.[19]

Figure 3(a) displays the VB-PES spectra of $CuCr_{1-x}O_2$ ($x = 0-0.1$) obtained with a photon energy of 150 eV. Striking differences were observed between the VB-PES spectra of the Cr-deficient samples with $x = 0.02-0.1$ and that of the Cr-deficiency-free sample, i.e., $x = 0$. Since the photoionization cross section of Cu 3d is four times as large as that of Cr 3d at an excitation photon energy of $h\nu = 150$ eV,[20] the three major features, A_4–C_4 in the spectra of $CuCr_{1-x}O_2$ shown in Fig. 3(a) are primarily attributable to Cu 3d and O 2p-Cu 3d hybridized states and O 2p bonding states,[8,9] although the valence band of $CuCrO_2$ is almost entirely composed of the Cr 3d states due to the strong hybridization between Cr 3d and O 2p orbitals.[6,10] Apparently, the intensity of feature C_4

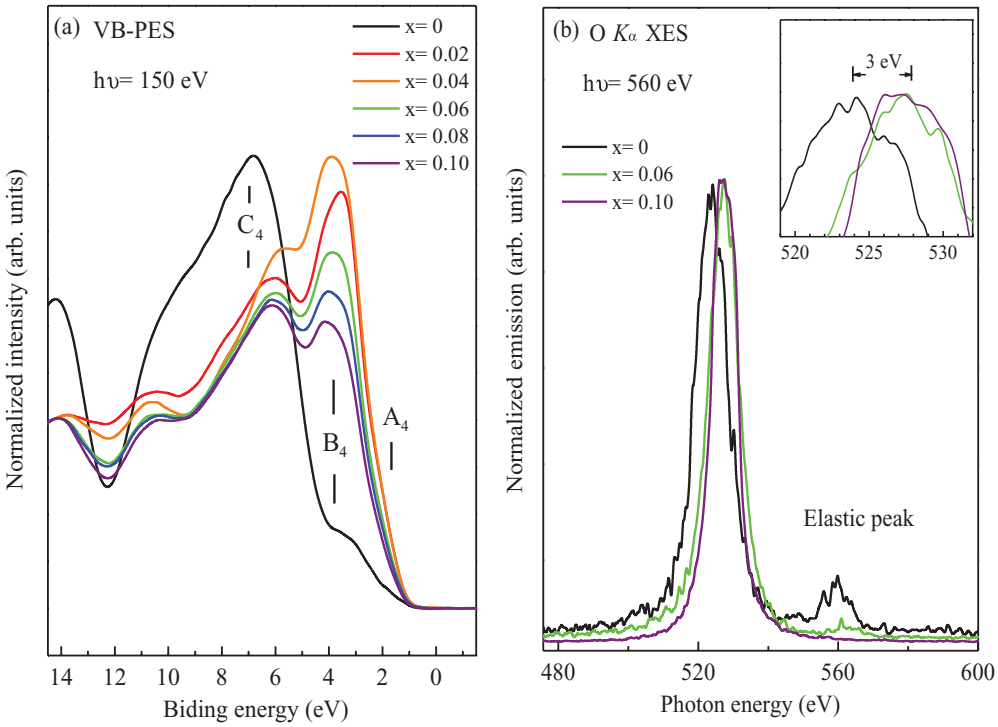

FIG. 3. (Color online) (a) VB-PES spectra of $CuCr_{1-x}O_2$ ($x = 0$–0.1). (b) O K_α XES spectra of $CuCr_{1-x}O_2$ ($x = 0$,0.06, and 0.1). The upper inset magnifies the main feature of the XES spectra. Note that a satellite feature at ~560 eV is an elastic peak.

of the samples with $x = 0.02$–0.1 is much lower than that of the sample with $x = 0$, and the intensities of features A_4 and B_4 are significantly higher. These changes indicate that the O $2p$ valence electrons shift to the more delocalized O $2p$-Cu $3d$ and localized Cu $3d$ states to create holes and to enhance the conductivity for the Cr-deficient samples. Figure 3(b) presents the O K_α XES spectra obtained at an excitation energy of 560 eV, which include a main feature centered at ~524 eV for $x = 0$ and 527 eV for $x = 0.06$ and 0.1 associated with the O $2p$ states below VBM or E_f. As x increases from 0 to 0.06 and 0.1, the feature associated with the O $2p$ states is shifted to the higher energy by ~3 eV as displayed in the upper inset of Fig. 3(b), suggesting the shift in the DOS of O $2p$ toward VBM or E_f. This shift is consistent with the VB-PES results shown in Fig. 3(a), which shows an ~3 eV shift from the intensity maximum of feature C_4 of the $x = 0$ sample to that of feature B_4 of the $x = 0.02$–0.1 samples. The overall drop in the intensities of features A_4 and B_4 with increasing Cr deficiency shown in Fig. 3(a) strongly indicates an increase in the number of Cr-deficiency-doped holes at the Cu sites, accompanied by a decrease in DOS at or near VBM or E_f.

To shed light on the temperature-dependent p-type electrical conduction in $CuCr_{1-x}O_2$, $\ln(\rho)$, as a function of temperature for samples studied, is displayed in Fig. 4(a). A deviation from T-linear behavior in the $\ln(\rho)$-T plot below ~250 K suggests that there is a crossover electrical conduction mechanism around 250 K. In the temperature region of ~250 K $< T <$ 300 K, experimental data fit well to straight dashed lines, indicative of a strong support of the thermally activated (TA) mechanism with $\rho(T) = \rho_0 \exp[(E_{TA}/kT)]$, where E_{TA} denotes the activation energy. The estimated E_{TA} value determined from the slopes of these straight lines increases from ~0.07 eV for the $x = 0.1$ sample to ~0.28 eV for the $x = 0$ sample as shown in the inset of Fig. 4(a). The values of E_{TA} are much smaller than the reported band gap (E_g) value of 2.95–3.30 eV,[11] indicating that the thermally excited electrons are transferred into shallow acceptor or defect states in the gap[21] as presented schematically in Fig. 4(b), rather than a conduction-band minimum (CBM). A higher Cr-deficiency sample with a smaller E_{TA} makes valence electrons easy to excite into the shallow acceptor or defect states. It correspondingly increases the number of holes in the valence band and gives rise to a higher conductivity. These findings not only agree with the reported results that the holes govern charge transport in $CuCr_{1-x}O_2$ compounds,[13] but also consistently reconcile the reduction in DOS at or near VBM or E_f and the increase in the Cu^{2+} valence state as x increases, discussed above. In the temperature region of ~130 K $< T <$ 250 K, $\rho(T)$ follows a combination of the TA and three-dimensional variable range hopping (3D-VRH) model with the expression $\rho(T) \propto \exp[E_{TA}/kT] + \exp[(T_0/T)^{1/4}]$ displayed in the solid curves in Fig. 4(a), where $T_0 \propto 1/a^3$ and a is the localization length of carriers.[22] It suggests that the Mott's VRH mechanism participates in charge transport between ~130 K and 250 K and the p-type conductivity is still partially contributed by thermally activated valence electrons that create holes in the valence band.

To get a better understanding of the temperature-dependent p-type conductivity in the $CuCr_{1-x}O_2$ samples, the temperature-dependent Cu $L_{3,2}$-edge XANES spectra of $CuCr_{1-x}O_2$ ($x = 0$, 0.06, and 0.1) and reference CuO and Cu_2O at RT are shown in the Supplementary Material of Figs. S3(a)–S3(c) in Ref. 4. They exhibit features similar to those of A_2/A_2^* and B_2/B_2^* in the Cu $L_{3,2}$-edge spectra

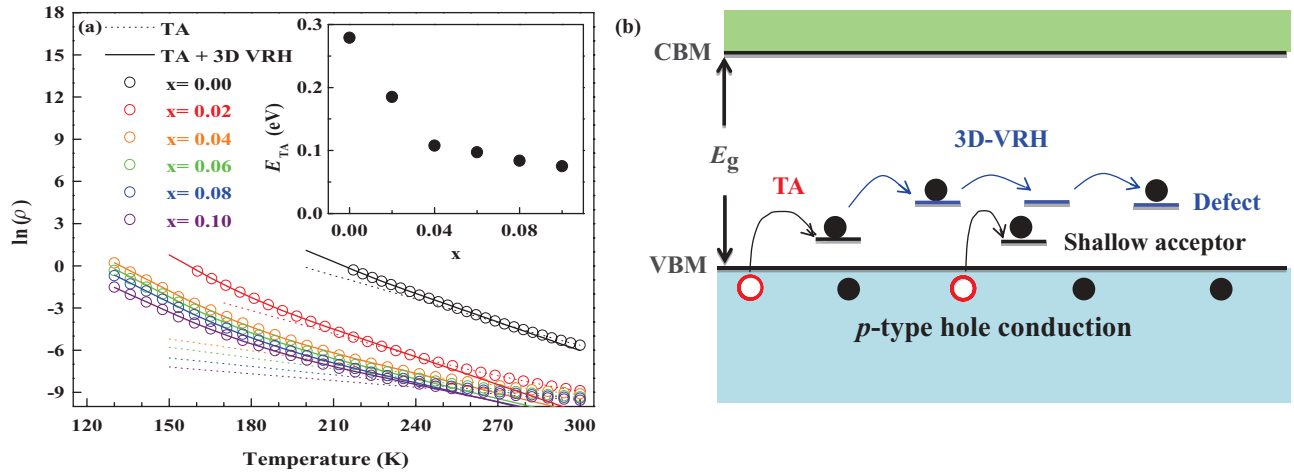

FIG. 4. (Color online) (a) ln(ρ) versus T for $CuCr_{1-x}O_2$ ($x = 0$–0.1): Open circles represent experimental data, dotted lines represent fitting by TA conduction, and solid lines represent fitting by a combination of the TA and 3D-VRH mechanisms. (b) A schematic illustrates the TA and 3D-VRH conductions.

shown in Fig. 1(b). As shown in the bottom panels of Figs. S3(a)–S3(c), the intensities of the Cu $L_{3,2}$ edge features overall decrease with decreasing temperature, indicative of a decrease in the number of unoccupied Cu 3d states. More interestingly, as temperature increased from 90 K up to RT, a gradual valence state change from Cu^{1+} to Cu^{2+} was observed for the $x = 0.06$ sample, in contrast, the amount of Cu^{1+} in the $x = 0$ sample, nearly kept constant, and that of Cu^{2+} in the $x = 0.1$ samples increased. This finding reveals that the p-type carrier conduction assisted by thermal excitation for samples with higher Cr deficiency becomes more pronounced at high temperatures. As a result, it increases the number of holes at the Cu/O sites, causing more Cu^{1+} to become Cu^{2+} and significantly enhances p-type conductivity at high temperatures. Additionally, according to the analysis of the EXAFS data [also see Figs. S4(a) and S4(b) in the Supplementary Material (Ref. 4)], no substantial variation in the Cu-O and Cu-Cu bond distances with x was observed in the $CuCr_{1-x}O_2$ samples. The result clearly suggests that the observed changes in the p-type conductivity over a wide range of temperatures predominantly arise from changes in the electronic structures not the Cu-O and Cu-Cu bond distances.

ACKNOWLEDGMENTS

This work was financially supported by National Science Council of Taiwan under Contracts No. NSC 99-2112-M-032-004-MY3 and No. NSC 99-2119-M-032-004-MY3.

*Present address: Department of Physics, National Taiwan University, Taiwan.

†Author to whom all correspondence should be addressed: dcling@mail.tku.edu.tw

‡wfpong@mail.tku.edu.tw

[1] S. Seki, Y. Onose, and Y. Tokura, Phys. Rev. Lett. **101**, 067204 (2008).

[2] K. Kimura, H. Nakamura, S. Kimura, M. Hagiwara, and T. Kimura, Phys. Rev. Lett. **103**, 107201 (2009).

[3] T. Arnold, D. J. Payne, A. Bourlange, J. P. Hu, R. G. Egdell, L. F. J. Piper, L. Colakerol, A. De Masi, P.-A. Glans, T. Learmonth, K. E. Smith, J. Guo, D. O. Scanlon, A. Walsh, B. J. Morgan, and G. W. Watson, Phys. Rev. B **79**, 075102 (2009).

[4] See Supplemental Material at http://link.aps.org/supplemental/10.1103/PhysRevB.86.241103 for more discussion and figures.

[5] R. Nagarajan, N. Duan, M. K. Jayaraj, J. Li, K. A. Vanaja, A. Yokochi, A. Draeseke, J. Tate, and A. W. Sleight, Int. J. Inorg. Mater. **3**, 265 (2001).

[6] A. Maignan, C. Martin, R. Frésard, V. Eyert, E. Guilmeau, S. Hébert, M. Poienar, and D. Pelloquin, Solid State Commun. **149**, 962 (2009).

[7] T. Okuda, N. Jufuku, S. Hidaka, and N. Terada, Phys. Rev. B **72**, 144403 (2005).

[8] D. O. Scanlon, A. Walsh, B. J. Morgan, G. W. Watson, D. J. Payne, and R. G. Egdell, Phys. Rev. B **79**, 035101 (2009).

[9] D. O. Scanlon, K. G. Godinho, B. J. Morgan, and G. W. Watson, J. Chem. Phys. **132**, 024707 (2010).

[10] R. Gillen and J. Robertson, Phys. Rev. B **84**, 035125 (2011).

[11] D. O. Scanlon and G. W. Watson, J. Mater. Chem. **21**, 3655 (2011).

[12] D. Shin, J. S. Foord, D. J. Payne, T. Arnold, D. J. Aston, R. G. Egdell, K. G. Godinho, D. O. Scanlon, B. J. Morgan, G. W. Watson, E. Mugnier, C. Yaicle, A. Rougier, L. Colakerol, P. A. Glans, L. F. J. Piper, and K. E. Smith, Phys. Rev. B **80**, 233105 (2009).

[13] D. C. Ling, C. W. Chiang, Y. F. Wang, Y. J. Lee, and P. H. Yeh, J. Appl. Phys. **109**, 07D908 (2011).

[14] C. B. Stagarescu, X. Su, D. E. Eastman, K. N. Altmann, F. J. Himpsel, and A. Gupta, Phys. Rev. B **61**, R9233 (2000).

[15] D. J. Huang, H.-T. Jeng, C. F. Chang, G. Y. Guo, J. Chen, W. P. Wu, S. C. Chung, S. G. Shyu, C. C. Wu, H.-J. Lin, and C. T. Chen, Phys. Rev. B **66**, 174440 (2002).

[16] L. H. Tjeng, C. T. Chen, and S. W. Cheong, Phys. Rev. B **45**, 8205 (1992).

[17]M. Karppinen, M. Kotiranta, T. Nakane, H. Yamauchi, S. C. Chang, R. S. Liu, and J. M. Chen, Phys. Rev. B **67**, 134522 (2003).

[18]M. Schneider, R.-S. Unger, R. Mitdank, R. Müller, A. Krapf, S. Rogaschewski, H. Dwelk, C. Janowitz, and R. Manzke, Phys. Rev. B **72**, 014504 (2005).

[19]S. W. Han, D. C. Ling, H. M. Tsai, C. H. Chuang, S. L. Wu, W. F. Pong, J. W. Chiou, M.-H. Tsai, L. Y. Jang, H. J. Lin, T. W. Pi, and J. F. Lee, Phys. Rev. B **85**, 014506 (2012).

[20]J. J. Yeh and I. Lindau, At. Data Nucl. Data Tables **32**, 1 (1985).

[21]C.-W. Pao, C.-T. Wu, H.-M. Tsai, Y.-S. Liu, C.-L. Chang, W. F. Pong, J.-W. Chiou, C.-W. Chen, M.-S. Hu, M.-W. Chu, L.-C. Chen, C.-H. Chen, K.-H. Chen, S.-B. Wang, S.-J. Chang, M.-H. Tsai, H.-J. Lin, J.-F. Lee, and J.-H. Guo, Phys. Rev. B **84**, 165412 (2011).

[22]N. F. Mott and E. A. Davis, *Electronic Processes in Non-Crystalline Materials* (Clarendon, Oxford, 1971).